

Kalman Filtering for PMU position angle retrieval and encoder data analysis

Gilberto Goracci (Feb 20th - Apr 20th, 2024)

June 26, 2024

Contents

1 Encoder Data Analysis	2
1.1 Unfiltered Encoder Data	2
1.2 Filtered Encoder Data	3
1.2.1 First Filtering	3
1.2.2 Second Filtering	3
1.3 Signal Reconstruction	5
2 Kalman Filter for position angle retrieval	5
2.1 Kalman Filter Workflow	6
2.2 Maxima Retrieval	8
2.3 Process Noise Matrix Determination	8
2.4 Angle Retrieval with Encoder Data	9
2.5 Results on Real Data	10
2.5.1 Angular Velocity Retrieval	10
2.5.2 Results with angle re-initialization	10
2.5.3 Results without angle re-initialization	11
2.5.4 Spikes-affected Measurements	11
3 First 2024 PMU BBM Cryogenic Run Preparation	14
4 Conclusions	14
5 Resources	14
Appendix A: Kalman Filter Theory	20

1 Encoder Data Analysis

Encoder data from the second PMU BBM cryogenic run of 2023 has been processed.

1.1 Unfiltered Encoder Data

The rotational frequencies of the three encoders (A, B, Z) have been retrieved from the raw data, determining the statistical properties of the frequency distributions (Fig. 1). The Fast Fourier Transform (FFT) of the encoder signals has been used to distinguish the main components in the frequency domain from spurious components (Fig. 2).

The origin of the spurious components in the frequency domain is still under investigation. The 50 Hz component with the relative harmonics has been associated with ground power supply.

It has been discovered that encoder A can show signs of malfunction, resulting in a mirroring of encoder Z signal. This is clear both from the output signal itself (Fig. 3) and from the FFTs of encoders A and Z (Fig. 4).

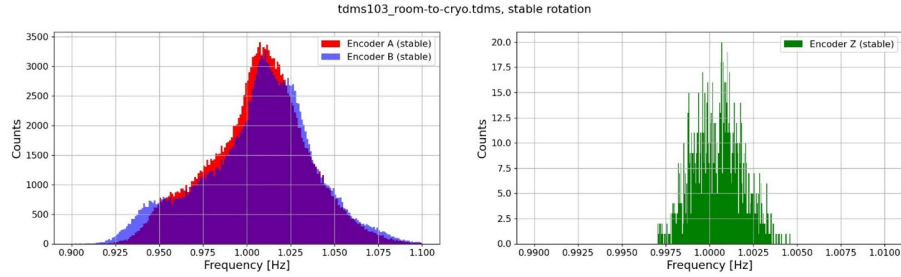


Figure 1: Encoders A, B (left) and Z (right) frequency histograms.

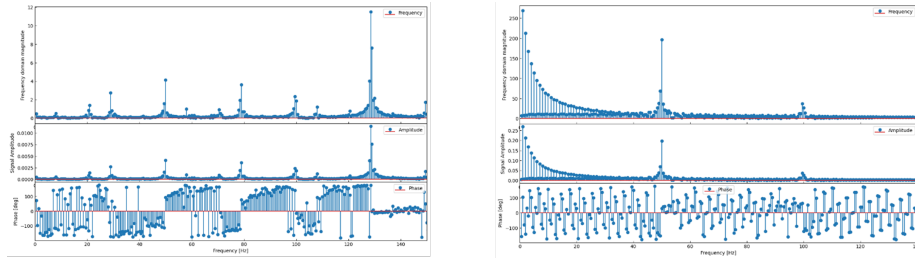


Figure 2: Encoder A/B (left) and Z (right) FFTs from the tdms103 data file. Different secondary amplitude peaks can be seen.

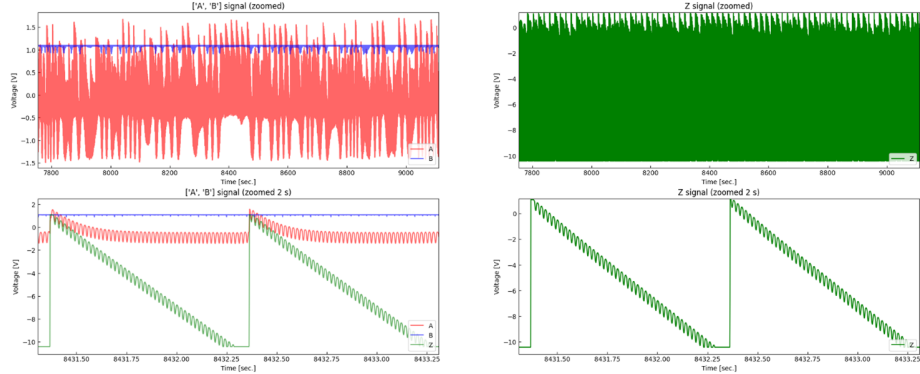


Figure 3: Encoder A, B, Z output signal (top row) and zoomed output signal (bottom row) from the tdms35 data file. Encoder A shows signs of malfunction and mirrors encoder Z.

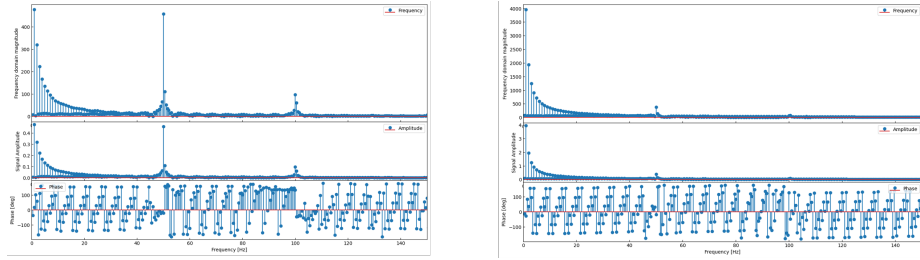


Figure 4: Encoder A and Z FFTs from the tdms35 data file. No peaks show around the expected frequency of 128 Hz for encoder A, while a substantial peak around 1 Hz (encoder Z expected frequency) is present.

1.2 Filtered Encoder Data

The encoder signal has been filtered to separate the main components in the frequency domain from spurious components.

1.2.1 First Filtering

In the first place, a band-pass filter between 120-130 Hz has been applied to encoders A and B, and a low-pass filter under 45 Hz to encoder Z. The new histograms of the frequency distribution are shown in Fig. 5.

1.2.2 Second Filtering

Here, encoder A and B signals have been filtered around 127-129 Hz and encoder Z signal around 0.99-1.01 Hz. Again, the resulting frequency distribution histograms are shown in Fig. 6.

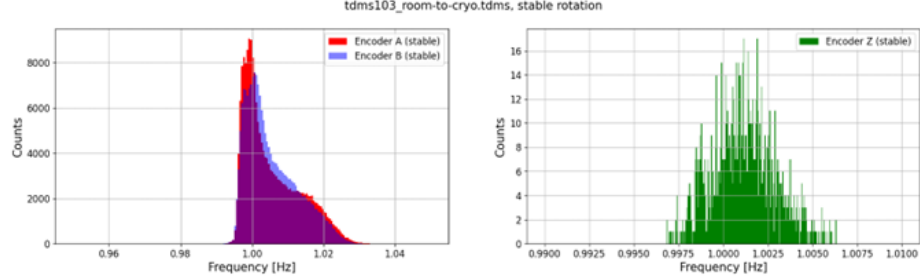


Figure 5: Encoders A, B (left) and Z (right) frequency histograms after the application of a 120-130 Hz band-pass filter and 45 Hz low-pass filter, respectively.

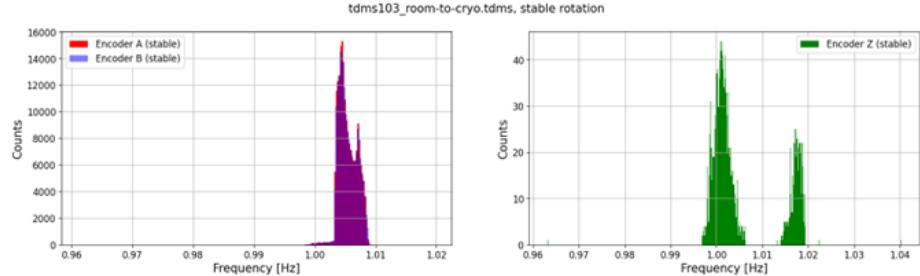


Figure 6: Encoders A, B (left) and Z (right) frequency histograms after the application of a 127-129 Hz and 0.99-1.01 Hz band-pass filter, respectively.

Table 1 shows the statistical properties of the frequency distributions before and after the filtering.

Encoder	Band [Hz]	Mean Frequency [Hz]	Std. Deviation [Hz]	$\frac{\sigma_{\text{freq}}}{f} [\%]$
A	[0, +inf)	1.006215675876	0.02864753861	2.85
B	[0, +inf)	1.006417898634	0.03214520274	3.19
Z	[0, +inf)	1.005403553614	0.00837585171	0.83
A	[120, 130]	1.005455407090	0.00776604551	0.77
B	[120, 130]	1.005390039057	0.00980555785	0.98
Z	[0, 45]	1.005443433348	0.00746250066	0.74
A	[127, 129]	1.0053960400920	0.00152705080	0.15
B	[127, 129]	1.0053953006919	0.00153585069	0.15
Z	[0.99, 1.01]	1.005443433348	0.00746250066	0.74

Table 1: Statistical properties of encoders frequency distributions.

1.3 Signal Reconstruction

An attempt to reconstruct the filtered signal from the tdms103 data file has been made using a square and a sine wave for encoders A and B and a Fourier series expansion up to 10 Hz for encoder Z. The free parameters of the model, such as amplitude and phase factors have been determined through maximum correlation with the real signals. These reconstructed signals have not been used later on in this analysis, but they might be worth seeing. Figure 7 shows the reconstructed signals for encoder A and B, while Fig. 8 shows a reconstruction of encoder Z signal superimposed to the actual data, for which the frequencies above 10 Hz have been filtered out. The residuals, namely the difference between the true and reconstructed signals, are shown in Figs. 9 and 10 for encoders A/B and Z, respectively.

The analytic expressions for the A and B sine waves are the following:

$$V_A(t) = A_A \sin(2\pi f_A t + \phi_A), \quad (1)$$

$$V_B(t) = A_B \sin(2\pi f_B t + \phi_B); \quad (2)$$

where:

- $A_A = 0.01333969922243$ V;
- $f_A = 128.690693131771$ Hz;
- $\phi_A = 4.05$ rad;
- $A_B = 0.01407871254636$ V;
- $f_B = 128.690598488559$ Hz;
- $\phi_B = 4.50$ rad.

The numerical values for the Fourier expansion of the reconstructed Z signal are not reported here. This is due to the heavy computational burden provided by such reconstruction, such that the parameters have been optimized only for a small sub-portion of data. For this reason, the numerical values do not add any useful information to this analysis.

Figures 9, in particular, and 10 show a periodic behaviour of the residuals. This aspect has not been investigated further.

2 Kalman Filter for position angle retrieval

A linear Kalman Filter (KF) has been implemented to reconstruct the position angle of the PMU in a real-time, onboard fashion. Technical details of the theory behind Kalman filtering can be found in Appendix A. At present time, the KF is applied only in the stable rotation phase of the PMU, and it processes each data point of the encoder signals one at a time, in order to recreate an onboard-like environment in which only one measurement is available at a time.

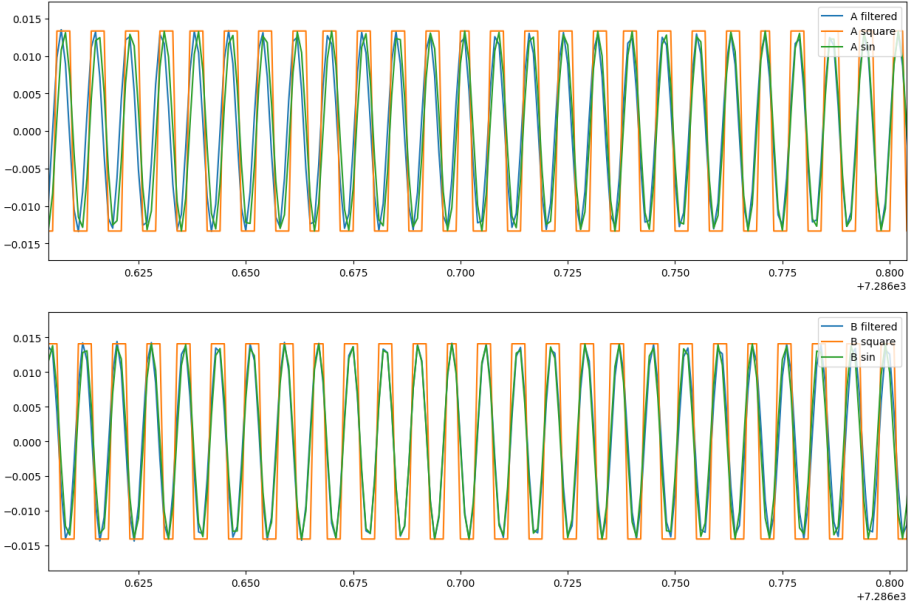


Figure 7: Reconstructed signal for encoders A (top) and B (bottom) using a square wave (orange line) and a sine wave (green line) over the true signal (blue line).

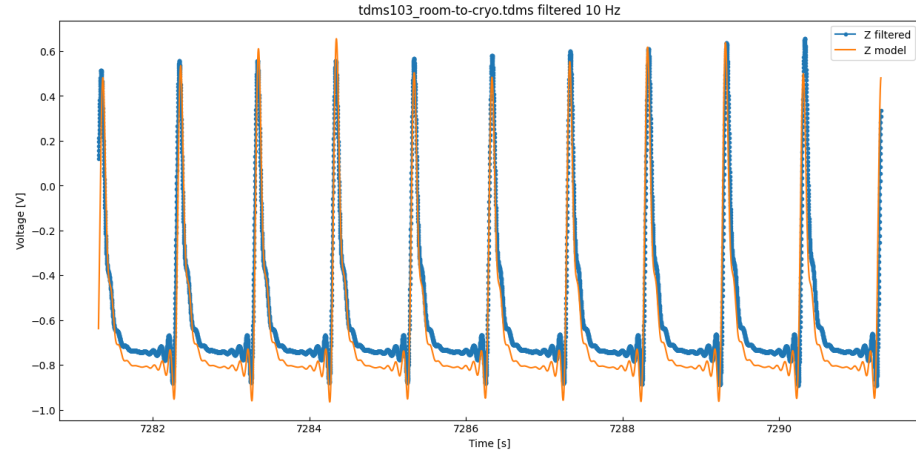


Figure 8: Reconstructed signal for encoder Z using a Fourier series expansion up to 10 Hz (orange line) over the true signal (blue line).

2.1 Kalman Filter Workflow

The workflow of the Kalman Filter is the following:

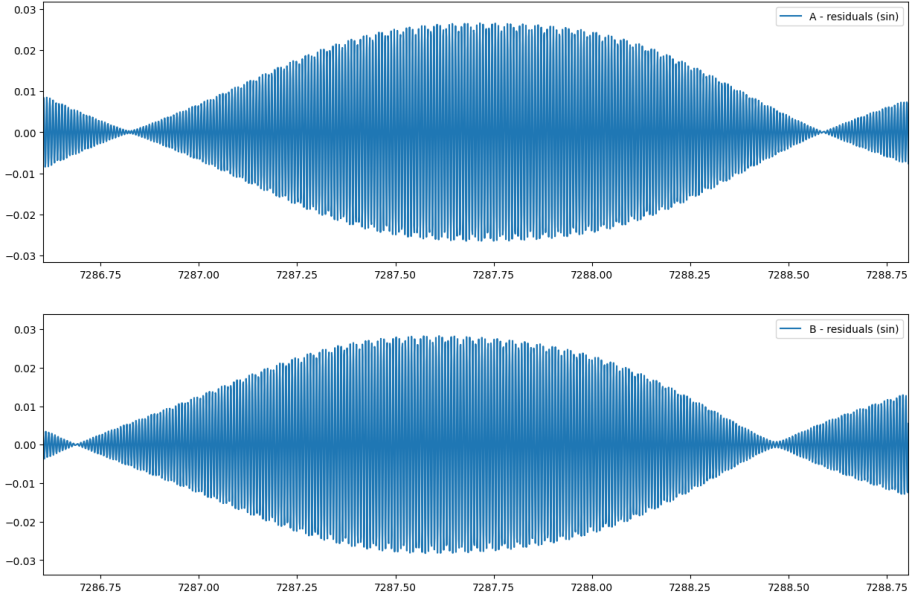


Figure 9: Residuals for the sine wave-reconstructed A (top) and B (bottom) signals.

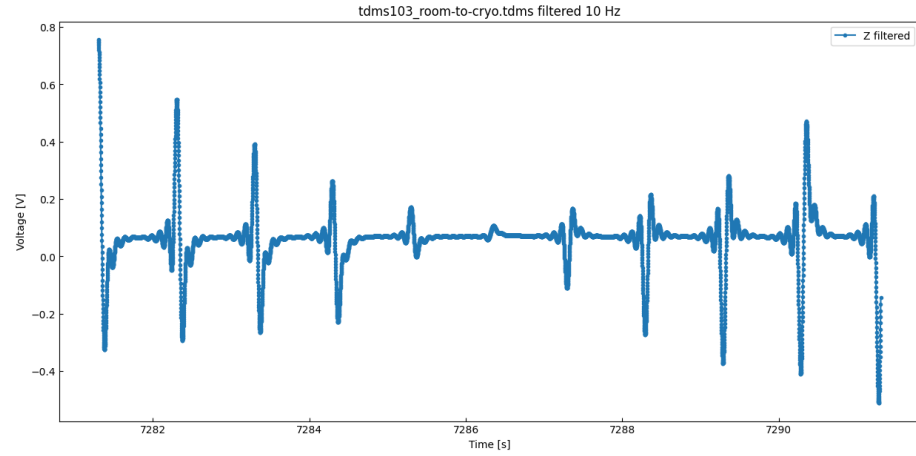


Figure 10: Residuals for the reconstructed Z signal.

- The state (angular position, velocity and acceleration) is initialized with null initial angle and acceleration and initial angular velocity set to 2π rad/s.
- The Z signal is inspected. The filtering begins when the signal is maxi-

mum. In this way a bit of information (from the start to the first Z peak) is lost, but the uncertainty on the initial position is removed, since the filter starts exactly at the reference zero.

- The angular velocity and acceleration are used to propagate the state forward in time until one of the three encoders exhibit a maximum in the signal.
- When a maximum in the signal is found, the KF is applied to retrieve the updates to the state.

2.2 Maxima Retrieval

As it is clear from this workflow, the determination of a maximum in the signal is crucial for the correct functioning of the filter. In particular, due to the real-time nature of the algorithm, this has to be done using the current and last measurements only, as storing the entirety of the data would exceed the memory capabilities of the payload. To do this, an algorithm based on the derivative of the signal has been created:

- A threshold for the data signal of each encoder is empirically determined. This threshold can be adjusted in real time to deal with long time scale variation in the data (such as $1/f$ noise).
- A window with a fixed width w is set for each encoder.
- Let x_t and x_{t-1} be two data points from an encoder signal.
- If $x_t \geq x_{t-1}$ then x_t is not a maximum.
- If $x_t < x_{t-1}$ then x_t is stored as a maximum provided that the following conditions are met:
 - The value of x_t is greater than the threshold set for that specific encoder.
 - At least w data points have been processed from the last maximum acquisition. This is done to correctly process rapidly oscillating signals and to avoid that each data point greater than the next one is considered as a maximum.

2.3 Process Noise Matrix Determination

The process noise matrix \mathbf{Q} of the KF has been tuned performing a Montecarlo Simulation of KF runs with different diagonal values for \mathbf{Q} and those minimizing the mean residual (the difference between the measured and propagated angle) throughout the run have been selected. The mean residuals for a 2-dimensional \mathbf{Q} are shown in Fig. 11.

The following results have been obtained with

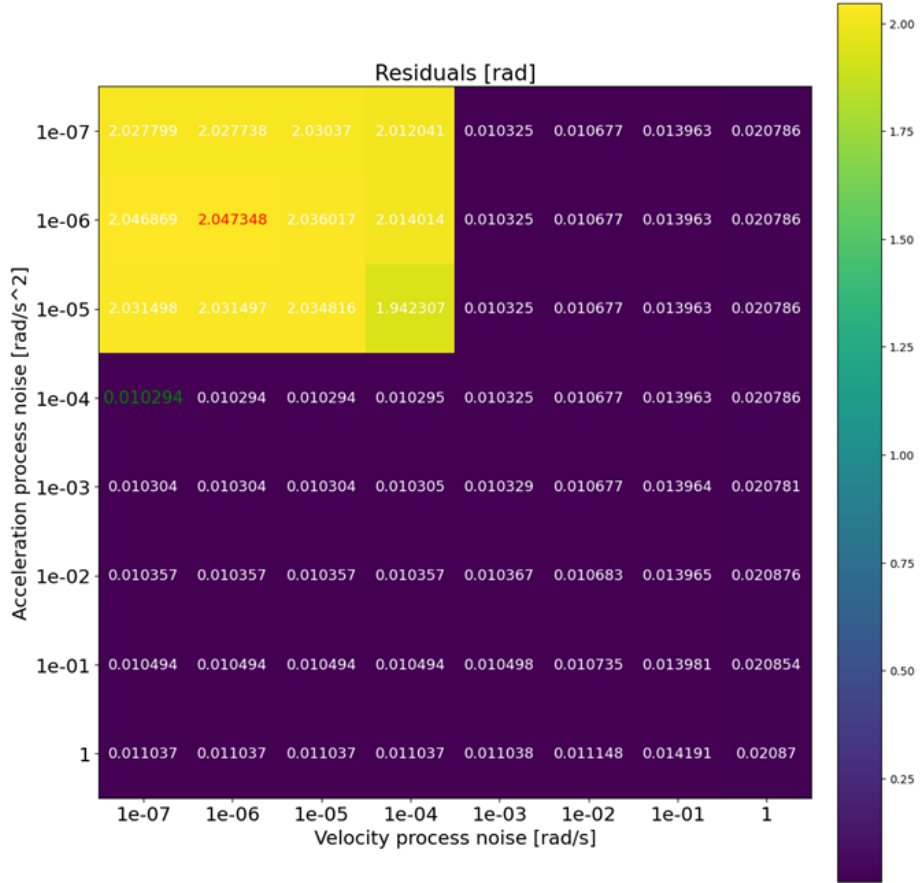


Figure 11: Montecarlo Simulation results with different two-dimensional process noise matrices \mathbf{Q} using the residuals as goodness measure of the Kalman Filter.

$$\mathbf{Q} = \begin{bmatrix} 10^{-14} & 0 & 0 \\ 0 & 10^{-6} & 0 \\ 0 & 0 & 10^{-14} \end{bmatrix}. \quad (3)$$

2.4 Angle Retrieval with Encoder Data

In parallel to the KF the position angle propagation has been made also using the three encoders separately. The working scheme of the encoder-based propagation is very simple: the angular velocity is derived from the time interval between two peaks in the signal of the chosen encoder and the update takes place when a maximum is processed, in the same fashion as the KF. In this way, the position angle can be propagated starting from the initial condition of

zero degrees.

The performance of this encoder-based tools depends on whether, when an angular measurement $\hat{\theta}_k$ is collected, the tool sets the position angle θ_k to the measurement, that is $\theta_k = \hat{\theta}_k$ and means that the measurement is 100% trusted by the algorithm. If this re-initialization of the angular position happens the tool proceeds smoothly, otherwise the residuals rapidly diverge, as Secs. 2.4 and 2.5.3 will show. However, there is a non-negligible margin of error when an angle is associated to a voltage measurement, therefore one does not want to rely on the angular measurement so much. Despite not properly being a filter, these algorithms will be referred to as "A-B-Z filters" hereafter, for simplicity.

2.5 Results on Real Data

A Kalman Filter (KF) has been used to process the encoder data in real time to retrieve the position angle of the PMU during the stable rotation phase. The results have been compared to the angular position and velocity retrieved using the A-B-Z filters described earlier.

With the same set of parameters, the KF can process all the data of the cryogenic run as long as A, B and Z encoders are present and working correctly. Moreover, the KF does not need angle re-initialization: this means that the angular measurements are exploited to compute the state updates but never trusted as being 100% correct.

Another point is that KF can handle the case of superimposed maxima (A and B at the same time), it will notice that there is a superimposition and discards the maximum corresponding to the last analyzed encoder (if the last processed measure comes from encoder A it will process B)

Residuals between the KF-reconstructed angle and the angle measurement (affected by error) have a mean of 0.0003 degrees and a standard deviation of 0.65 degrees. In absence of true angle values the residuals give the best estimation of the filter performance. Considering the distribution of the squared residuals, the mean is 0.42 squared degrees and the standard deviation is 0.33 squared degrees.

2.5.1 Angular Velocity Retrieval

KF showed less dispersion in the computed frequencies (Fig. 12) with respect to the A-B-Z filters. The frequency is linked to the angular velocity of the PMU by a factor 2π . For the A-B-Z filters the frequencies are correctly computed with or without angle re-initialization.

2.5.2 Results with angle re-initialization

The KF and A-B-Z filters residuals as a function of time are shown in Fig. 13, where the angle is re-initialized at every collected measurement for the A-B-Z filters according to Sec. 2.4. The histogram of the residuals distribution is

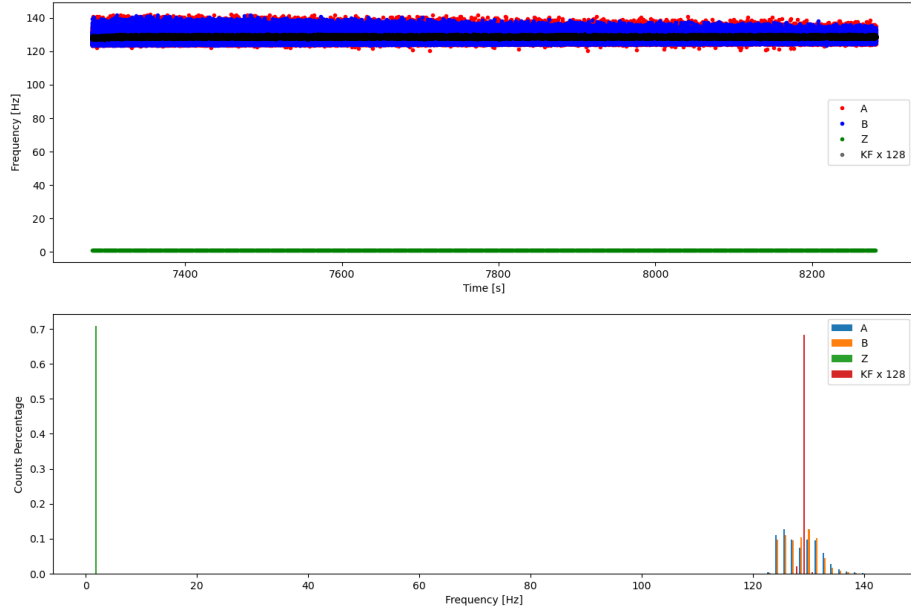


Figure 12: Kalman Filter- and A-B-Z filters-derived rotor frequency as a function of time (top) and histogram (bottom) during the stable rotation phase.

shown in Fig. 14. Finally, Fig. 15 shows the angular position retrieved with the KF and the A-B-Z filters in a 5 seconds-long time window.

2.5.3 Results without angle re-initialization

The KF and A-B-Z filters residuals as a function of time are shown in Fig. 13, where no angle re-initialization is performed for the A-B-Z filters. The histogram of the residuals distribution is shown in Fig. 14. Finally, Fig. 15 shows the angular position retrieved with the KF and the A-B-Z filters in a 5 seconds-long time window.

It is clear from the figures that the A-B-Z filters rapidly diverge without angle re-initialization, and therefore are not to be considered reliable if the uncertainty on the angular measurement is not negligible.

2.5.4 Spikes-affected Measurements

This section shows the results of the KF when the encoder data has been contaminated by spikes in the signal. Such anomalies in the data can be caused, for example, by a cosmic ray crossing the detector and, therefore, need to be handled by the readout system. For this analysis rates up to 0.1 spikes per second have been considered, which is a realistic limit for the expected spikes per second ratio. The spikes have been simulated as a very high voltage value

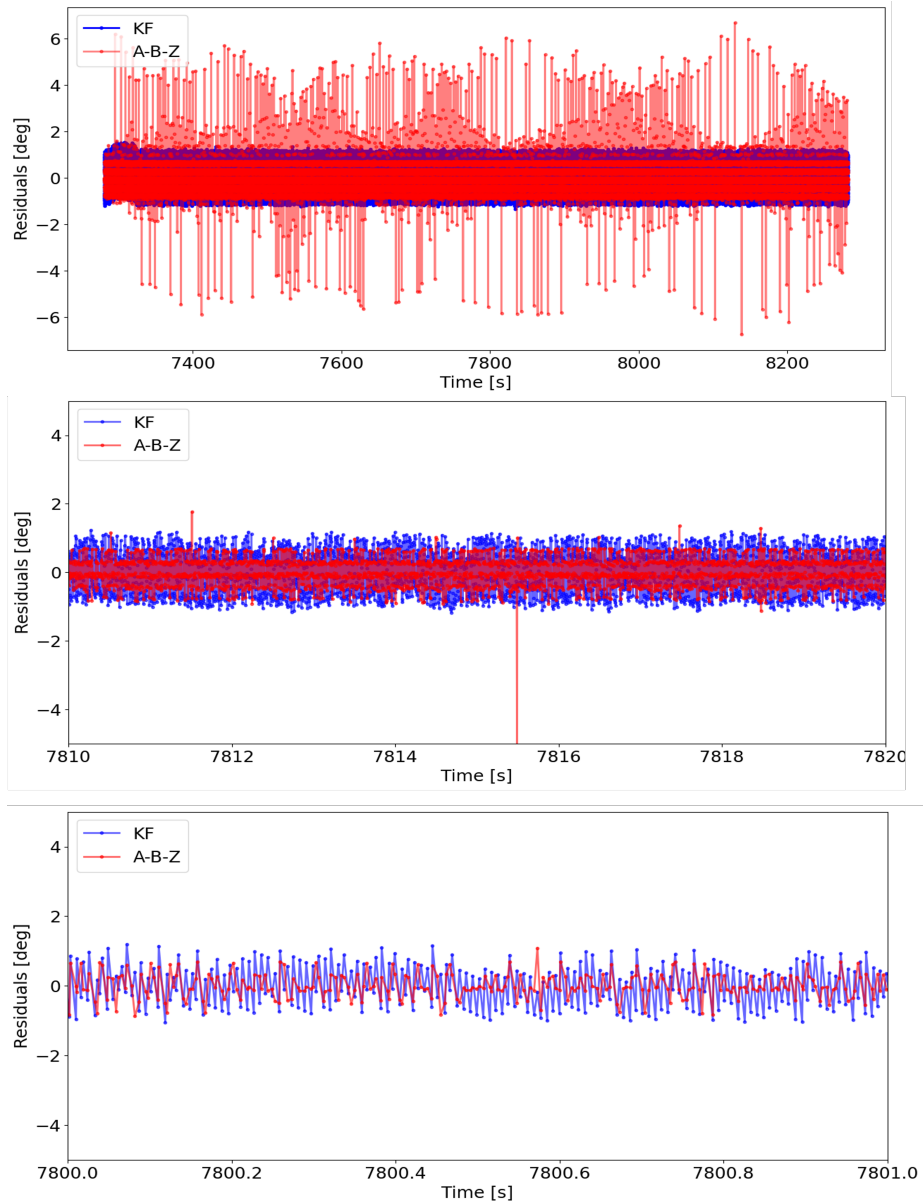


Figure 13: Kalman Filter and A-B-Z filters residuals with angle re-initialization. First row: stable rotation phase, second row: 10 seconds-long time window, third row: one second-long time window.

detected by one encoder randomly chosen between A, B and Z. Completely similar results are expected if the anomaly is detected by two or more encoders at

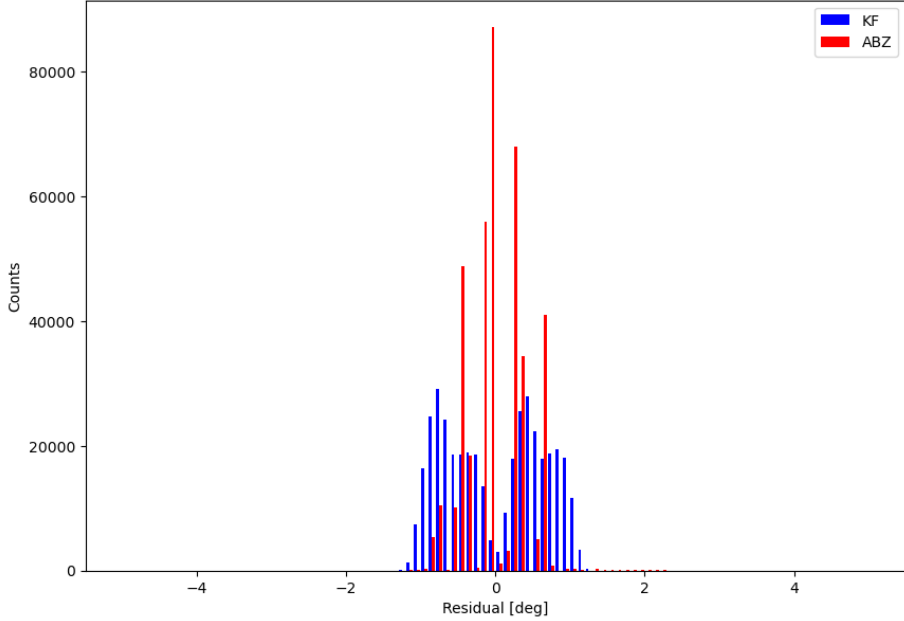


Figure 14: Kalman Filter and A-B-Z filters residuals histogram with angle re-initialization.

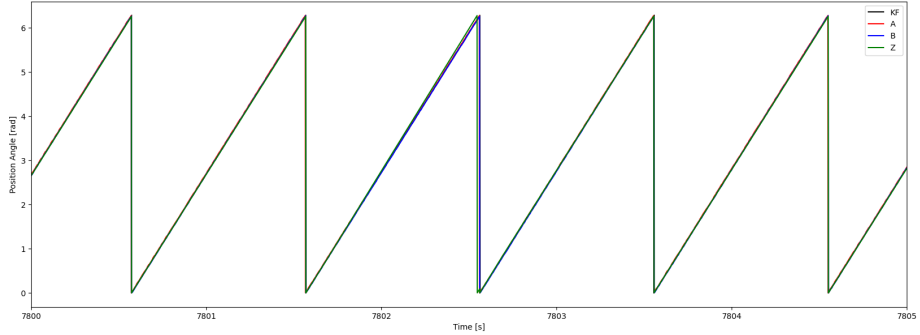


Figure 15: Kalman Filter- and A-B-Z filters-retrieved rotor angular position with angle re-initialization.

the same time.

The frequencies and the angular position in time are shown in Figs. 19 and 20, respectively. The figures show that the KF is able to restore its operational workflow and, subsequently, the correct angular position with the considered spikes per second rates. For higher rates the same results are not guaranteed and the KF ultimately diverges with particularly high rates. The anomalies in the KF-retrieved rotor frequency and angular position correspond to the

detection of a spike.

3 First 2024 PMU BBM Cryogenic Run Preparation

As of April 2024, a new PMU BBM cryostat run has begun, and new data is being collected. Involvements on this matter include the soldering and assembly of a new encoder set, a set of OP-amplifiers to connect to the read-out system of the encoder data and a touch probe to measure the temperature of the gripper inside the cryostat.

4 Conclusions

In this work, the encoder data from the second PMU BBM cryogenic run of 2023 has been analyzed. In the first part of the work the statistical properties of the rotor frequency distribution has been investigated, using unfiltered and filtered encoder data. The filtering has been done isolating the main frequency components of the encoder data identified using the Fast Fourier Transform of the signal. In the second part of the visiting period, a Kalman Filter has been used to process the raw encoder data in order to retrieve the angular position of the rotor in real time. The KF has shown consistent and stabler results compared with and encoder-based position angle retrieval. However, the absolute accuracy of the filter is still under investigation and needs to be assessed from tests on simulated data.

Future developments of this work include:

- Test the KF to retrieve the position angle outside of the stability region (i.e. when the rotor is accelerating). A preliminary step in this direction has been made and the results seem promising, but more work has to be done. In particular, an attempt to retrieve the rotational frequency throughout the entire data file has been successfully made (Fig. 21), however a set of parameters compatible with all the data files is still to be determined and the performance in terms of angular position is not satisfactory at all.
- Test how the KF performs using only two encoders or one encoder alone.
- As mentioned above, asses the accuracy of the KF from simulated encoder data.

5 Resources

The Python scripts used in this work are available at <https://github.com/braseg257/KF-for-PMU>. A more "hands on" guide in .pdf format about how the KF is applied

to the PMU is available at the same link and includes an explanation of the numerical values used in the scripts. The guide also illustrates how the voltage signal is "converted" into angular measurements. Please contact to the Kavli IPMU CMB Group staff to access the data files from the cryogenic BBM PMU runs.

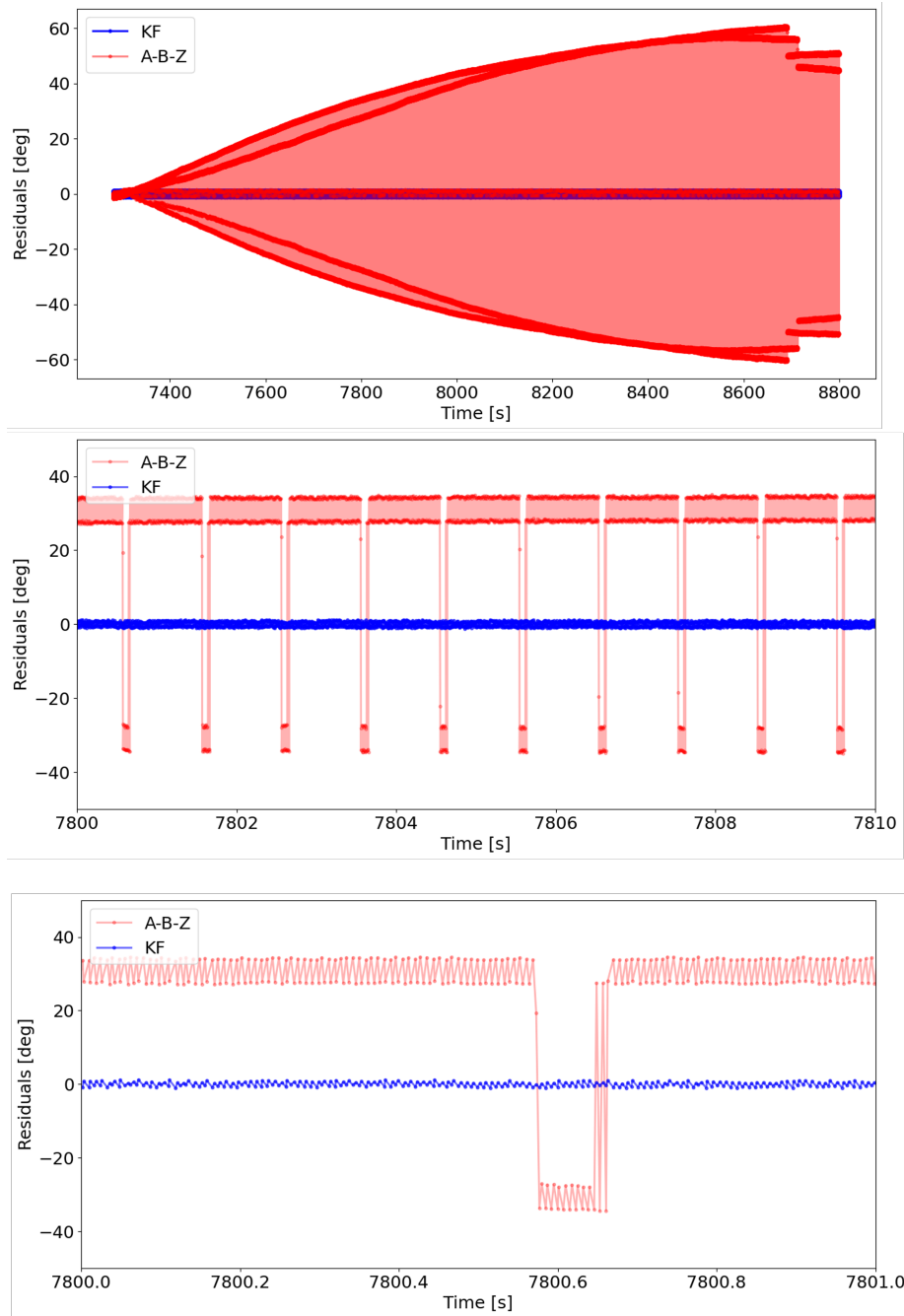


Figure 16: Kalman Filter and A-B-Z filters residuals without angle re-initialization. First row: stable rotation phase, second row: 10 seconds-long time window, third row: one second-long time window.

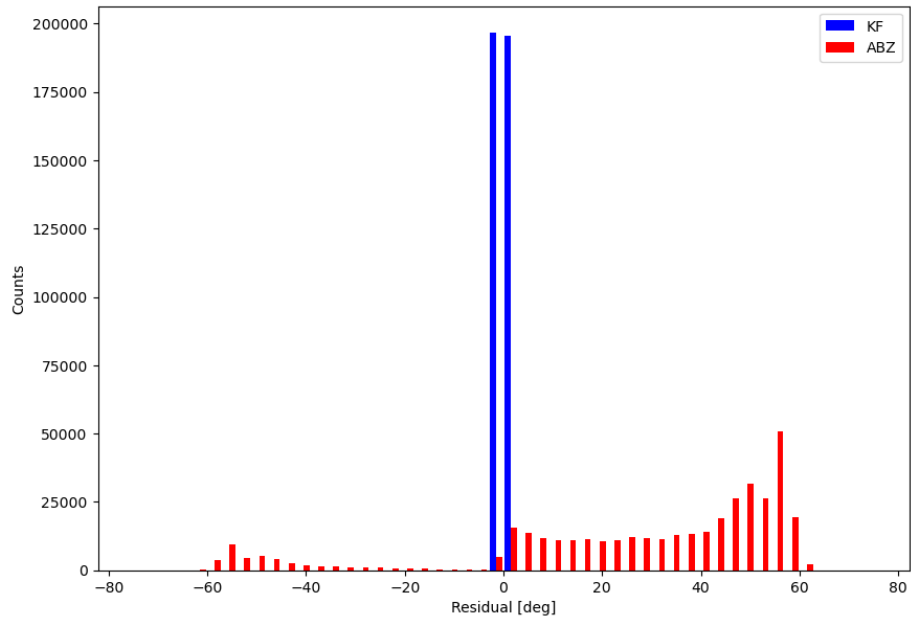


Figure 17: Kalman Filter and A-B-Z filters residuals histogram without angle re-initialization.

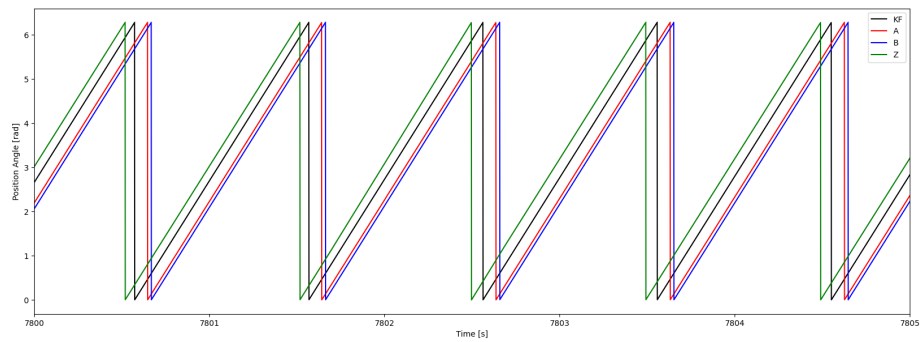


Figure 18: Kalman Filter- and A-B-Z filters-retrieved rotor angular position without angle re-initialization.

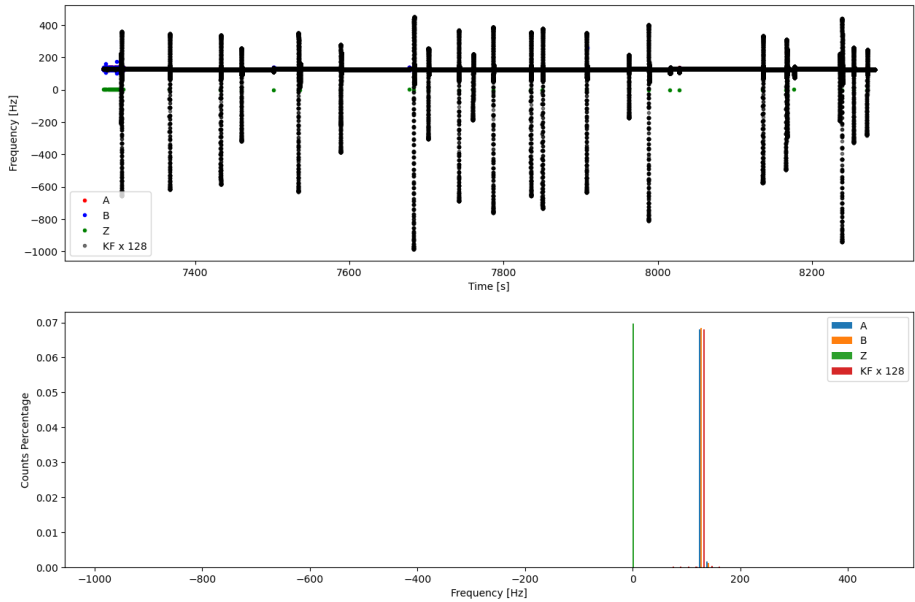


Figure 19: Kalman Filter- and A-B-Z filters-retrieved rotor frequency as a function of time (top) and histogram (bottom) with spikes-affected encoder data.

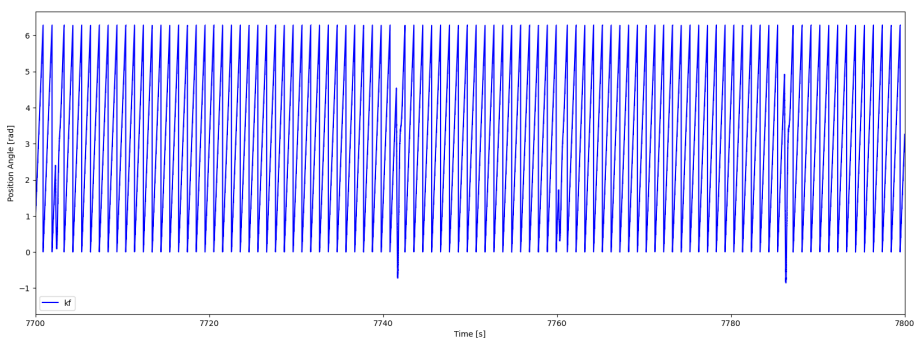


Figure 20: Kalman Filter-retrieved rotor angular position in time with spikes-affected encoder data.

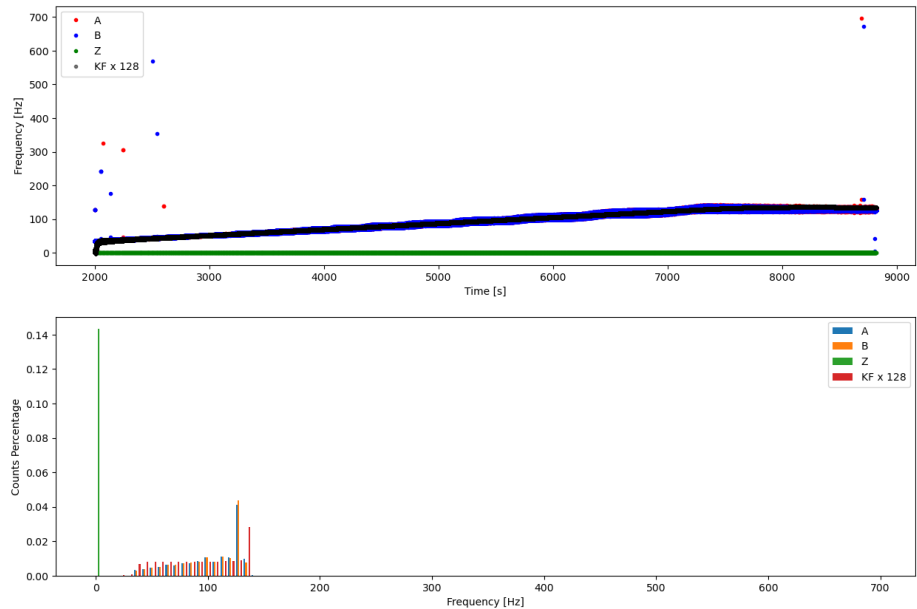


Figure 21: Kalman Filter- and A-B-Z filters-retrieved rotor frequency as a function of time throughout all the tdms103 data file.

Kalman Filter Theory

The Kalman Filter (KF) is a Model Based (MB) algorithm developed in the early 1960s. The quality of its performance is strictly linked to the knowledge of the underlying dynamics and to the goodness of model assumptions.

This appendix is mainly taken from the KF theory described by Zarchan, P. and Musoff, H. in the book *Fundamentals of Kalman Filtering: A Practical Approach, Third Edition*. Please check the book for more details.

To apply Kalman filtering theory, the model of the real world must be described by a set of differential equations. These equations must be cast in matrix or state-space form as

$$\dot{\mathbf{x}} = \mathbf{F}(\mathbf{x}) + \mathbf{w}. \quad (4)$$

where \mathbf{x} is a column vector with the states of the system, \mathbf{F} is the system dynamics matrix and \mathbf{w} is a white-noise process, which is also expressed as a vector. A process noise matrix \mathbf{Q} is related to the process-noise vector according to

$$\mathbf{Q} = E(\mathbf{w}\mathbf{w}^T), \quad (5)$$

where $E(\cdot)$ is the expected value operator.

The process noise matrix does not always have a physical meaning. Sometimes, it is used as a parameter to give the filter an indication of the goodness of the model of real world that is being used (see Sec. 2.3).

The KF formulation requires that the measurements are linearly related to the state, according to

$$\mathbf{o} = \mathbf{H}\mathbf{x} + \mathbf{v} \quad (6)$$

Where \mathbf{o} is the measurement vector, \mathbf{H} is the measurement matrix, and \mathbf{v} is a white measurement noise, which is also expressed as a vector. Similarly to the process noise, a measurement noise matrix \mathbf{R} is related to the measurement noise vector \mathbf{v} according to

$$\mathbf{R} = E(\mathbf{v}\mathbf{v}^T). \quad (7)$$

Here, the state vector \mathbf{x}_k at the k -th time step is represented by the angular position, velocity and acceleration of the rotor:

$$\mathbf{x}_k = [\theta, \dot{\theta}, \ddot{\theta}]^T, \quad (8)$$

while the observation vector \mathbf{o}_k is given by the angular measurement:

$$\mathbf{o}_k = \theta \quad (9)$$

and:

$$v = \frac{\frac{2\pi}{512}}{3} rad \quad (10)$$

The two matrices \mathbf{F} and \mathbf{H} are given by:

$$\mathbf{F} = \begin{bmatrix} 0 & 1 & 0 \\ 0 & 0 & 1 \\ 0 & 0 & 0 \end{bmatrix}, \quad (11)$$

and

$$\mathbf{H} = [1, 0, 0]. \quad (12)$$

The new state estimate $\hat{\mathbf{x}}_{k+1}$ is given by the following equation according to the KF theory:

$$\hat{\mathbf{x}}_{k+1} = \bar{\mathbf{x}}_{k+1} + \mathbf{K}_{k+1}[\mathbf{o}_{k+1} - \mathbf{H}\bar{\mathbf{x}}_{k+1}], \quad (13)$$

where $\bar{\mathbf{x}}_{k+1}$ is the state prediction, \mathbf{K} indicates the *Kalman gain* matrix, and $[\mathbf{o}_{k+1} - \mathbf{H}\bar{\mathbf{x}}_{k+1}]$ is the residual: the difference between the actual measurement and the non-linear measurement prediction.

In the case of discrete measurements Eq. (6) and (7) can be rewritten as:

$$\mathbf{o}_k = \mathbf{H}\mathbf{x}_k + \mathbf{v}_k. \quad (14)$$

and

$$\mathbf{R}_k = E(\mathbf{v}_k \mathbf{v}_k^T), \quad (15)$$

respectively.

The Kalman gain matrix can be computed from the Riccati equations, a set of recursive matrix equations given by:

$$\mathbf{M}_k = \Phi_k \mathbf{P}_{k-1} \Phi_k^T + \mathbf{Q}_k \quad (16)$$

$$\mathbf{K}_k = \mathbf{M}_k \mathbf{H}^T (\mathbf{H} \mathbf{M}_k \mathbf{H}^T + \mathbf{R}_k)^{-1} \quad (17)$$

$$\mathbf{P}_k = (\mathbf{I} - \mathbf{K}_k \mathbf{H}) \mathbf{M}_k, \quad (18)$$

where Φ_k is the *fundamental matrix* and can be approximated by the first two or three terms of the Taylor-series expansion of $e^{\mathbf{FT}_s}$: $\Phi_k \simeq I + \mathbf{FT}_s + \frac{1}{2}\mathbf{F}^2 T_s^2$, with T_s being the sampling time interval. The discrete process-noise matrix \mathbf{Q}_k can be computed as:

$$\mathbf{Q}_k = \int_0^{T_s} \Phi(\tau) \mathbf{Q} \Phi^T(\tau) d\tau. \quad (19)$$

Finally, the state prediction is given by:

$$\bar{\mathbf{x}}_{k+1} = \Phi_k \hat{\mathbf{x}}_k. \quad (20)$$

It is easy to verify that Eq. 20 yields the time law of a uniformly accelerated angular motion.

In the specific case of this analysis, when the application of the KF is limited to the stable rotation phase, the dimension of the state can be reduced to 2, neglecting the acceleration. If so, the underlying dynamics will be reduced to a linear angular motion and only the first two terms of Φ_k are needed.